*American Mineralogist, Volume 73, pages 1114–1119, 1988*

# High-pressure structure of anorthite

**R. J. Angel**
Geophysical Laboratory, 2801 Upton Street, N.W., Washington D.C. 20008, U.S.A.

## Abstract

The crystal structure of anorthite, $CaAl_2Si_2O_8$, has been determined by refinement to single-crystal X-ray diffraction data collected at 1 bar, 25 kbar, and 31 kbar. Over this pressure range there are no significant reductions in Al–O or Si–O bond lengths, and no significant changes in O–T–O bond angles. The phase transition at about 26.1 kbar is accompanied by the almost complete disappearance of *c* and *d* reflections, suggesting that the high-pressure phase has $I\bar{1}$ symmetry. Further evidence for this symmetry change is provided by the structural analysis based upon the data set collected at 31 kbar that shows single sites for the Ca atoms, in contrast to the split sites observed in the $I\bar{1}$ refinements of the low-pressure phase. The mechanism of the phase transition may be described as the tilting of essentially rigid tetrahedra.

## Introduction

Plagioclase feldspars are among the most abundant minerals within the Earth's crust. Yet until recently, their remarkably diverse subsolidus behavior has defied understanding, despite the potential use of plagioclase feldspars for geobarometry and geothermometry. The recent studies by Carpenter and co-workers (e.g., Carpenter et al., 1985; Carpenter, 1986) allied with the application of Landau theory (e.g., Salje, 1987; Redfern and Salje, 1987) has resulted in the development of a unified picture of the thermodynamic behavior of plagioclase feldspars, at least at ambient pressures (see review by Carpenter, 1988).

What has yet to be determined is the effect of pressure upon these complex phase relations. As a first step, Angel et al. (1988) measured the compressibilities of the end-member feldspars albite, sanidine, and anorthite by single-crystal X-ray diffraction methods in a diamond-anvil cell. These measurements prompted perhaps more questions than they answered, in that a predicted monoclinic → triclinic phase transition in sanidine was not detected, while significant metrical discontinuities indicated a phase transition in anorthite between 25.5 and 29.5 kbar. Subsequent work (Angel and Ross, 1988) has placed this transition at 26.1 ± 0.6 kbar.

The structure of all feldspars consists of a three-dimensional framework of corner-linked tetrahedra (Fig. 1) that contain Al and Si atoms. The complexity of feldspar structures arises in part from the interplay between Al,Si ordering among these tetrahedra and displacive distortions of the framework as a whole. The high-pressure phase transition in anorthite clearly belongs to this second type of transition, as it is readily reversible at room temperature in the diamond-anvil cell. This paper reports the results of a structural study of anorthite carried out at pressures above and below the transformation boundary and determines the structural changes associated with the phase transition.

## Experimental details

The anorthite used in this study is from the Val Pasmeda locality in Austria, and has been fully characterized by Carpenter et al. (1985). Crystals are reported as having variable composition between 99.5% and 100% anorthite component (Adlhart et al., 1980; Redfern and Salje, 1987). Thermodynamic analysis (Carpenter, 1988) suggests that the Al,Si distribution is about 95% ordered; certainly there is insufficient disorder to be detectable by $^{29}$Si MAS NMR (Kirkpatrick et al., 1987). A sample from the same locality was used for a single-crystal X-ray structure determination at ambient conditions by Wainwright and Starkey (1971).

A single crystal of approximate dimensions 60 × 60 × 80 μm, free from twins and optical imperfections, was selected on the basis of X-ray diffraction peak profiles collected on a diffractometer. A room-temperature and pressure data collection was carried out with a conventional glass-fiber mount before the crystal was mounted in a Merrill-Bassett type diamond-anvil cell. The pressure medium used was a 4:1 methanol : ethanol mixture, and pressure was determined by using the $R_1$ laser-induced fluorescence from a ruby chip included in the cell. A Picker four-circle diffractometer equipped with a Mo X-ray tube (β-filtered) was used for all the data collections. Unit cells were determined both before and after each data collection by centering between 10 and 12 accessible reflections in the range $20° < 2\theta < 25°$ by the method of King and Finger (1979). Intensities of all accessible reflections (*a, b, c,* and *d* type) in one-half of reciprocal space were collected with ω step-scans of 1° total width and a step size of 0.025°, with a count time of 10 s per step. Cell parameters and other crystallographic data are reported in Table 1.

Data collections were initially carried out at 25 and 31 kbar. But because of the limitations imposed upon accessible reflections by the geometry of the diamond-anvil cell and the orientation of the crystal, it was found that these data sets provided insufficient resolution along the *b* axis to allow stable structure

0003–004X/88/0910–1114$02.00

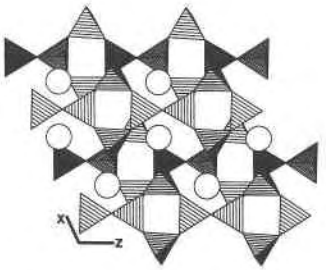


Fig. 1. A portion of the structure of anorthite viewed approximately down the *b* axis. Large circles represent Ca atoms.

refinements to be carried out. The diamond-anvil cell was therefore reloaded after these initial data collections with the crystal rotated into an orientation that allowed access to reflections with high *k* indices. Two further data collections were carried out with this new orientation at pressures as close as possible to those of the first data collections, as indicated by the cell parameters. The estimated differences in pressure between each pair of data collections are around 1 kbar.

Integrated intensities were obtained from the step-scans by a modified Lehmann-Larsen algorithm (Grant and Gabe, 1978), with the option to reset backgrounds interactively. An effort was made to ensure that only the Bragg intensity was integrated, and any diffuse background was excluded. Intensities were corrected for diamond absorption and Lp effects, but no correction was made for absorption by the feldspar crystal itself ($\mu_{calc} = 15$ cm$^{-1}$). Refinements to structure factors were carried out with the RFINE4 program (Finger and Prince, 1974) using the robust-resistant method of weighting individual reflections. Duplicated structure factors from the pairs of data collections were not averaged, as it was found that the individual data sets required slightly different scale factors.[1]

The diffraction pattern of anorthite at ambient conditions con-

[1] Tables of observed and calculated structure factors may be obtained by ordering document AM-88-387 from the Business Office, Mineralogical Society of America, 1625 I Street, N.W., Suite 414, Washington, D.C. 20006, U.S.A. Please remit $5.00 in advance for the microfiche.

TABLE 1. Crystal data for Val Pasmeda anorthite

| | 1 bar | 25 kbar | 31 kbar |
|---|---|---|---|
| *a* (Å) | 8.175(1) | 8.082(2) | 8.042(1) |
| *b* (Å) | 12.873(1) | 12.767(3) | 12.748(1) |
| *c* (Å) | 14.170(1) | 14.032(4) | 13.964(2) |
| $\alpha$ (°) | 93.11(1) | 92.79(3) | 92.20(1) |
| $\beta$ (°) | 115.89(1) | 115.77(2) | 115.27(1) |
| $\gamma$ (°) | 91.28(1) | 91.68(2) | 92.65(1) |
| *V* (Å$^3$) | 1337.8(2) | 1300.3(6) | 1290.5(2) |
| *R** | 7.1 | 13.0 | 11.7 |
| $R_w$* | 5.0 | 6.0 | 6.2 |
| $G_{fit}$ | 3.7 | 5.3 | 4.5 |
| $N_{par}$ | 114 | 114 | 106 |
| $N_{obs}$, $I > 3\sigma_I$ | 1822 | 1187 | 1430 |
| $N_{obs}$, *b* | 668 | 278 | 518 |
| $2\theta_{max}$ (°) | 50 | 65 | 65 |

*Note:* Numbers in parentheses are the estimated standard deviations ($1\sigma$) in the last decimal place given. This convention applies to all subsequent tables.

* *R* values refer to refinements in space group $I\bar{1}$ to *a* and *b* reflections alone.

TABLE 2a. Positional and thermal parameters from $I\bar{1}$ refinement of Val Pasmeda anorthite at 1 bar

| Site | *x* | *y* | *z* | $B_{iso}$ |
|---|---|---|---|---|
| Mooo* | 0.2644(4) | 0.9860(3) | 0.0864(3) | 1.08(6) |
| Mzoo* | 0.2687(4) | 0.0323(2) | 0.5435(2) | 0.16(5) |
| Moio* | 0.7738(4) | 0.5360(2) | 0.5416(2) | 0.60(5) |
| Mzio* | 0.7632(4) | 0.5038(3) | 0.0754(3) | 1.17(6) |
| T1oo | 0.0077(3) | 0.1574(2) | 0.1042(2) | 0.49(3) |
| T1oz | 0.0026(3) | 0.1635(2) | 0.6123(2) | 0.46(3) |
| T1mo | −0.0007(3) | 0.8145(2) | 0.1198(2) | 0.54(3) |
| T1mz | 0.0052(3) | 0.8178(1) | 0.6117(2) | 0.52(3) |
| T2oo | 0.6884(3) | 0.1125(2) | 0.1596(2) | 0.69(4) |
| T2oz | 0.6763(3) | 0.1050(2) | 0.6568(1) | 0.64(3) |
| T2mo | 0.6752(3) | 0.8810(2) | 0.1806(2) | 0.64(3) |
| T2mz | 0.6838(3) | 0.8746(2) | 0.6771(2) | 0.49(3) |
| Oa1o | 0.0072(7) | 0.1239(4) | −0.0086(4) | 1.31(9) |
| Oa1z | 0.9987(7) | 0.1251(4) | 0.4905(4) | 1.44(9) |
| Oa2o | 0.5739(6) | 0.9891(3) | 0.1392(3) | 0.78(8) |
| Oa2z | 0.5723(6) | 0.9906(3) | 0.6380(3) | 0.69(8) |
| Oboo | 0.8250(7) | 0.0984(4) | 0.0928(4) | 1.27(9) |
| Oboz | 0.7986(8) | 0.1000(4) | 0.5927(4) | 1.41(9) |
| Obmo | 0.8066(8) | 0.8551(4) | 0.1266(4) | 1.9(1) |
| Obmz | 0.8274(8) | 0.8548(4) | 0.6182(4) | 1.9(1) |
| Ocoo | 0.0116(6) | 0.2778(4) | 0.1344(4) | 0.84(8) |
| Ocoz | 0.0129(6) | 0.2938(4) | 0.6481(4) | 0.96(9) |
| Ocmo | 0.0088(6) | 0.6794(4) | 0.1075(4) | 0.71(8) |
| Ocmz | 0.0075(6) | 0.6921(4) | 0.5995(4) | 0.87(8) |
| Odoo | 0.1904(7) | 0.1066(4) | 0.1854(4) | 1.17(9) |
| Odoz | 0.2029(7) | 0.1035(4) | 0.6929(4) | 1.53(9) |
| Odmo | 0.1979(7) | 0.8692(4) | 0.2213(4) | 1.8(1) |
| Odmz | 0.1871(8) | 0.8634(4) | 0.7086(5) | 2.4(1) |

* All M positions comprise 0.5 Ca atom each.

TABLE 2b. Positional and thermal parameters from $I\bar{1}$ refinement of Val Pasmeda anorthite at 25 kbar

| Site | *x* | *y* | *z* | $B_{iso}$ |
|---|---|---|---|---|
| Mooo* | 0.263(1) | 0.987(1) | 0.0862(8) | 0.6(1) |
| Mzoo* | 0.264(1) | 0.028(1) | 0.5422(9) | 0.2(2) |
| Moio* | 0.774(1) | 0.539(1) | 0.5407(9) | 0.8(2) |
| Mzio* | 0.759(1) | 0.506(1) | 0.0742(8) | 0.4(2) |
| T1oo | 0.0096(9) | 0.1569(8) | 0.1032(6) | 0.4(1) |
| T1oz | −0.0011(9) | 0.1641(9) | 0.6132(6) | 0.4(1) |
| T1mo | −0.002(1) | 0.8120(9) | 0.1189(7) | 0.6(1) |
| T1mz | 0.0043(9) | 0.8180(9) | 0.6120(6) | 0.5(1) |
| T2oo | 0.691(1) | 0.114(1) | 0.1634(6) | 0.6(1) |
| T2oz | 0.6688(9) | 0.101(1) | 0.6527(6) | 0.8(1) |
| T2mo | 0.671(1) | 0.8807(9) | 0.1819(6) | 0.6(1) |
| T2mz | 0.679(1) | 0.8722(9) | 0.6743(6) | 0.5(1) |
| Oa1o | 0.013(2) | 0.118(2) | −0.007(1) | 1.4(4) |
| Oa1z | −0.007(2) | 0.128(2) | 0.488(1) | 1.2(4) |
| Oa2o | 0.568(2) | 0.989(2) | 0.137(1) | 0.8(3) |
| Oa2z | 0.571(2) | 0.988(2) | 0.641(1) | 0.2(3) |
| Oboo | 0.824(2) | 0.092(2) | 0.092(1) | 1.6(4) |
| Oboz | 0.802(2) | 0.103(2) | 0.595(2) | 1.8(4) |
| Obmo | 0.812(3) | 0.855(2) | 0.128(2) | 1.9(4) |
| Obmz | 0.816(3) | 0.853(2) | 0.615(2) | 2.4(4) |
| Ocoo | 0.008(2) | 0.273(2) | 0.135(1) | 1.1(3) |
| Ocoz | 0.006(2) | 0.294(2) | 0.648(1) | 0.6(3) |
| Ocmo | 0.009(2) | 0.681(2) | 0.108(1) | 0.8(3) |
| Ocmz | 0.003(2) | 0.690(2) | 0.599(1) | 1.1(3) |
| Odoo | 0.187(2) | 0.100(2) | 0.183(1) | 1.6(4) |
| Odoz | 0.206(3) | 0.108(2) | 0.692(2) | 1.9(4) |
| Odmo | 0.187(3) | 0.865(2) | 0.223(2) | 2.8(5) |
| Odmz | 0.198(3) | 0.868(2) | 0.708(2) | 2.9(5) |

* All M positions comprise 0.5 Ca atom each.

TABLE 2c. Positional and thermal parameters from $I\bar{1}$ refinement of Val Pasmeda anorthite at 31 kbar

| Site | x | y | z | $B_{iso}$ |
|---|---|---|---|---|
| Mooo | 0.2682(4) | 0.0348(4) | 0.0401(3) | 0.44(6) |
| Mzoo | 0.2653(5) | 0.0055(4) | 0.5767(3) | 0.80(7) |
| T1oo | 0.0050(6) | 0.1565(6) | 0.1033(3) | 0.32(8) |
| T1oz | 0.9966(7) | 0.1601(6) | 0.6136(4) | 0.6(1) |
| T1mo | 0.9988(7) | 0.8106(7) | 0.1209(4) | 0.4(1) |
| T1mz | 0.0036(7) | 0.8163(6) | 0.6111(4) | 0.63(9) |
| T2oo | 0.6862(7) | 0.1108(6) | 0.1673(4) | 0.39(7) |
| T2oz | 0.6700(6) | 0.1027(6) | 0.6498(4) | 0.39(9) |
| T2mo | 0.6685(6) | 0.8789(6) | 0.1739(4) | 0.38(8) |
| T2mz | 0.6815(7) | 0.8731(6) | 0.6842(4) | 0.5(1) |
| Oa1o | 0.982(1) | 0.126(1) | 0.9838(9) | 0.4(2) |
| Oa1z | 0.023(1) | 0.126(1) | 0.4966(8) | 0.4(2) |
| Oa2o | 0.564(1) | 0.985(1) | 0.1346(9) | 0.4(2) |
| Oa2z | 0.574(1) | 0.991(1) | 0.6454(9) | 0.3(2) |
| Oboo | 0.833(1) | 0.092(1) | 0.1071(9) | 0.7(2) |
| Oboz | 0.782(1) | 0.097(1) | 0.5762(9) | 0.4(2) |
| Obmo | 0.787(1) | 0.858(1) | 0.1081(8) | 0.3(2) |
| Obmz | 0.840(1) | 0.848(1) | 0.6372(9) | 0.6(2) |
| Ocoo | 0.006(1) | 0.282(1) | 0.135(1) | 1.1(2) |
| Ocoz | 0.015(1) | 0.288(1) | 0.6534(9) | 0.9(2) |
| Ocmo | 0.996(1) | 0.676(1) | 0.1061(9) | 0.9(2) |
| Ocmz | 0.006(1) | 0.691(1) | 0.601(1) | 1.0(2) |
| Odoo | 0.201(1) | 0.110(1) | 0.1750(9) | 0.7(2) |
| Odoz | 0.188(1) | 0.094(1) | 0.6974(9) | 0.5(2) |
| Odmo | 0.179(1) | 0.862(1) | 0.234(1) | 1.2(2) |
| Odmz | 0.207(1) | 0.868(1) | 0.698(1) | 0.9(2) |

tains all four classes of reflections (*a, b, c, d*) indicative of a unit cell with $P\bar{1}$ symmetry. All four classes of reflections persisted at 25 kbar with approximately the same relative intensities ($a > c > b > d$). However, owing to the large number of parameters and low numbers of observed *b, c,* and *d* reflections, correlation problems developed in the refinement of a structure with $P\bar{1}$ symmetry to the 25-kbar data set. Therefore, the refinements of the structures at 1 bar and 25 kbar reported here are of an average structure with $I\bar{1}$ symmetry refined to the *a* and *b* reflections alone. A full refinement of the 1-bar data will be reported elsewhere (Angel, Finger, and Carpenter, unpub. ms., 1988) as part of a study of structural variation in anorthite-rich feldspars.

Atom coordinates from the $I\bar{1}$ refinement of a disordered plagioclase (Facchinelli et al., 1979) were used as an initial model for the 1-bar and 25-kbar refinements, and complex atomic scattering factors for neutral atoms were taken from the *International Tables for X-ray Crystallography* (1974). Scale factors, positional parameters, and isotropic temperature factors were refined to *a* and *b* reflections alone in space group $I\bar{1}$, but with the Ca atoms modeled as split sites in the structures determined at 1 bar and 25 kbar. Degradation of data quality by the diamond-anvil cell precludes the refinement of anisotropic temperature factors, and the 1-bar structure was refined in the same way as those at high pressure for the purposes of comparison. A discussion of the effect of the use of anisotropic temperature factors upon refined parameters can be found in Angel, Finger, and Carpenter (unpub. ms., 1988). Final agreement indices for the 1-bar and 25-kbar refinements are given in Table 1, and atomic coordinates from these two refinements are given in Tables 2a and 2b.

The diffraction pattern of anorthite above the transition shows a change in the relative intensities of the various classes of reflections, with $a > b \gg c, d$. Indeed, the very few *c* and *d* reflections observed in the data collections at 31 kbar were extremely diffuse and may well be of similar origin to those observed at temperatures above the $P\bar{1} \rightarrow I\bar{1}$ transition in anorthite at ambient pressures (Adlhart et al., 1980). Structure refinement was attempted in space group $I\bar{1}$ using the 1-bar refined structure as an initial model. However, the refinement did not converge while the residuals for the *b* reflections were disproportionately larger than those of the *a* reflections, even when allowing for the weaker intensities of the former. This indicated that although the average structure represented by the *a* reflections was correct, the symmetry breaking of this $C\bar{1}$ average structure which gives rise to the *b* reflections was being modeled incorrectly. Structure solution was therefore attempted by direct methods using a pair of unsplit Ca atoms (Mooo and Mzoo) to phase the observed structure factors. This enabled the positions of the tetrahedral cations to be identified, and further cycles of phasing using all of the cation positions resulted in the location of the oxygen

TABLE 3a. Tetrahedral bond lengths from $I\bar{1}$ refinements

| | 1 bar | 25 kbar | 31 kbar | | 1 bar | 25 kbar | 31 kbar |
|---|---|---|---|---|---|---|---|
| T1oo–Oa1o | 1.631(5) | 1.607(21) | 1.629(12) | T1oz-Oa1z | 1.757(5) | 1.775(20) | 1.777(11) |
| –Oboo | 1.600(5) | 1.636(21) | 1.597(13) | –Oboz | 1.742(5) | 1.665(25) | 1.722(13) |
| –Ocoo | 1.582(5) | 1.532(26) | 1.642(18) | –Ocoz | 1.716(5) | 1.699(25) | 1.683(18) |
| –Odoo | 1.615(5) | 1.604(18) | 1.618(11) | –Odoz | 1.761(6) | 1.724(19) | 1.762(11) |
| Avg. | 1.607 | 1.595 | 1.622 | Avg. | 1.744 | 1.724 | 1.736 |
| T1mz–Oa1z | 1.647(5) | 1.605(15) | 1.635(11) | T1mo–Oa1o | 1.780(5) | 1.815(16) | 1.756(11) |
| –Obmz | 1.578(6) | 1.611(20) | 1.570(10) | –Obmo | 1.710(6) | 1.675(19) | 1.769(10) |
| –Ocmz | 1.620(5) | 1.632(28) | 1.605(18) | –Ocmo | 1.749(5) | 1.678(27) | 1.716(18) |
| –Odmz | 1.591(6) | 1.644(26) | 1.654(15) | –Odmo | 1.730(6) | 1.681(28) | 1.702(17) |
| Avg. | 1.609 | 1.623 | 1.616 | Avg. | 1.742 | 1.712 | 1.728 |
| T2oz–Oa2z | 1.633(5) | 1.585(25) | 1.575(17) | T2oo–Oa2o | 1.770(5) | 1.792(27) | 1.785(18) |
| –Oboz | 1.618(5) | 1.605(16) | 1.632(10) | –Oboo | 1.758(5) | 1.771(18) | 1.738(11) |
| –Ocmo | 1.604(5) | 1.593(21) | 1.627(12) | –Ocmz | 1.739(5) | 1.745(20) | 1.746(12) |
| –Odmo | 1.589(5) | 1.644(27) | 1.590(16) | –Odmz | 1.698(6) | 1.624(24) | 1.704(15) |
| Avg. | 1.611 | 1.607 | 1.606 | Avg. | 1.741 | 1.733 | 1.743 |
| T2mo–Oa2o | 1.637(5) | 1.646(22) | 1.612(14) | T2mz–Oa2z | 1.755(5) | 1.722(22) | 1.754(15) |
| –Obmo | 1.599(6) | 1.653(19) | 1.607(10) | –Obmz | 1.728(6) | 1.672(19) | 1.704(11) |
| –Ocoz | 1.605(5) | 1.593(23) | 1.576(16) | –Ocoo | 1.730(5) | 1.728(25) | 1.664(17) |
| –Odoz | 1.624(6) | 1.611(22) | 1.681(14) | –Odoo | 1.760(5) | 1.821(22) | 1.780(14) |
| Avg. | 1.616 | 1.626 | 1.619 | Avg. | 1.743 | 1.736 | 1.725 |
| Avg. Si–O | 1.611 | 1.613 | 1.616 | Avg. Al–O | 1.735 | 1.726 | 1.733 |
| Avg. T–O | 1.677 | 1.670 | 1.674 | | | | |

TABLE 3b. Ca–O bond lengths less than 3.0 Å from $I\bar{1}$ refinements

| | 1 bar | 1 bar | 25 kbar | 25 kbar | 31 kbar |
|---|---|---|---|---|---|
| | Mooo | Moio | Mooo | Moio | Mooo |
| Oa1o | 2.710(6) | 2.320(5) | 2.596(19) | 2.212(19) | 2.454(10) |
| Oa1o | 2.388(6) | 2.912(6) | 2.349(27) | 2.878(24) | 2.712(15) |
| Oa2o | 2.302(5) | 2.343(5) | 2.247(17) | 2.293(19) | 2.307(10) |
| Oboo | 2.493(5) | 2.348(5) | 2.443(25) | 2.291(29) | 2.386(16) |
| Obmo | | 2.667(6) | | 2.616(19) | 2.417(10) |
| Ocmz | | 2.578(5) | | 2.483(30) | 2.542(17) |
| Odoo | 2.300(5) | 2.546(5) | 2.222(25) | 2.494(22) | 2.354(13) |
| Odmo | 2.718(6) | | 2.789(20) | | |
| Avg. | 2.485 | 2.531 | 2.441 | 2.467 | 2.453 |
| $V$ (Å$^3$) | 28.5 | | 27.0 | | 28.9 |
| | Mzoo | Mzio | Mzoo | Mzio | Mzoo |
| Oa1z | 2.373(5) | 2.578(6) | 2.403(19) | 2.570(18) | 2.440(11) |
| Oa1z | 2.809(5) | 2.477(6) | 2.713(24) | 2.436(27) | 2.592(15) |
| Oa2z | 2.340(5) | 2.298(5) | 2.346(18) | 2.301(16) | 2.268(10) |
| Oboz | 2.367(5) | 2.508(6) | 2.347(29) | 2.531(26) | 2.337(14) |
| Obmz | 2.611(6) | | 2.589(20) | | |
| Ocmo | 2.522(5) | 2.870(7) | 2.571(28) | 2.849(24) | 2.693(17) |
| Odoz | 2.534(5) | 2.276(6) | 2.551(24) | 2.241(25) | 2.305(13) |
| Odmz | | 2.925(7) | | 2.823(21) | 2.641(12) |
| Avg. | 2.508 | 2.562 | 2.503 | 2.536 | 2.468 |
| $V$ (Å$^3$) | 27.5 | | 26.3 | | 28.3 |

atoms. Subsequent refinement using this as an initial model was successful, resulting in the agreement indices reported in Table 1 and the atomic coordinates listed in Table 2c. Attempts to replace the single Ca atoms of the initial model with split sites analogous to those resulting from the 1-bar and 25-kbar refinements were unsuccessful, with each pair coalescing back into a single atom. The reasons for this are discussed below.

## DISCUSSION

In well-ordered end-member anorthite the tetrahedra are alternately occupied by Al and Si atoms in such a way as to give every $SiO_4$ tetrahedron four $AlO_4$ nearest-neighbors, and vice versa. The ordering of Al and Si atoms reduces the symmetry of the structure from $C$–face centered with $c \approx 7$ Å, to $I$-centered with $c \approx 14$ Å. It is this ordering, together with its accompanying structural distortions, that gives rise to the $b$ reflections in anorthite diffraction patterns. Further distortions of this framework reduce the symmetry to $P\bar{1}$ at low temperatures (below 240 °C in Val Pasmeda anorthite; Wruck, 1986) and results in the $c$ and $d$ reflections.

The structure determination at 1 bar therefore represents an average structure in which each atom (except the Ca positions) is used to model two atoms in the true structure which are nearly, but not quite, related by an $I$-lattice vector, ½,½,½. Thus, the bond lengths and angles reported in Tables 3 and 4 are not the true values, but are a kind of average of those that would be determined in a $P\bar{1}$ refinement of the structure. The exception is the case of the Ca atoms that occupy the larger cavities within the tetrahedral framework. The amount by which pseudo-$I$ related pairs of Ca positions violate the $I\bar{1}$ symmetry in the $P\bar{1}$ structure is sufficient to allow them to be distinguished (as half-atom split sites) even in an $I\bar{1}$ refinement. Figures 2a and 2d show the observed scattering density at the two symmetrically distinct Ca sites at 1 bar and clearly demonstrate the "split" nature of the site arising from the averaging in space group $I\bar{1}$.

The $I\bar{1}$ structure refined to the data collected at 25 kbar is essentially the same as that at 1 bar, although the poorer data quality arising from the effect of diamond absorption on the weaker reflections (only 278 $b$ reflections were observed) has resulted in very much larger esd's for all parameters. Average tetrahedral bond distances (Table

TABLE 4a. O–T–O bond angles from $I\bar{1}$ refinements

| | $O_A$–$O_B$ | $O_A$–$O_C$ | $O_A$–$O_D$ | $O_B$–$O_C$ | $O_B$–$O_D$ | $O_C$–$O_D$ |
|---|---|---|---|---|---|---|
| | | | 1 bar | | | |
| T1oo | 101.9(3) | 117.3(3) | 101.7(3) | 111.5(2) | 113.2(3) | 110.7(3) |
| T1oz | 98.1(2) | 119.1(2) | 97.8(3) | 112.8(2) | 116.0(3) | 111.9(3) |
| T1mo | 102.7(2) | 112.7(2) | 102.7(3) | 114.0(3) | 113.3(3) | 110.6(2) |
| T1mz | 103.2(3) | 113.2(3) | 105.0(3) | 112.2(3) | 113.0(3) | 110.0(3) |
| T2oo | 104.5(2) | 101.7(2) | 107.1(2) | 113.4(2) | 112.6(3) | 116.1(3) |
| T2oz | 107.1(3) | 102.1(2) | 109.8(3) | 113.0(3) | 110.3(3) | 114.1(3) |
| T2mo | 110.1(3) | 105.0(2) | 108.7(3) | 112.1(3) | 108.7(3) | 112.3(3) |
| T2mz | 109.7(2) | 105.1(2) | 105.2(2) | 111.1(2) | 110.5(3) | 114.9(2) |
| | | | 25 kbar | | | |
| T1oo | 100.7(1.3) | 122.1(1.2) | 99.0(1.0) | 110.8(1.1) | 108.8(1.1) | 113.9(1.2) |
| T1oz | 98.3(1.2) | 118.1(1.0) | 97.0(1.0) | 111.9(1.1) | 118.8(1.2) | 111.7(1.2) |
| T1mo | 99.8(0.9) | 116.0(1.1) | 105.2(1.1) | 116.0(1.2) | 108.9(1.4) | 110.1(1.2) |
| T1mz | 104.2(0.9) | 112.0(1.2) | 101.4(1.1) | 110.4(1.3) | 116.7(1.4) | 111.7(1.2) |
| T2oo | 99.9(1.2) | 97.8(1.0) | 106.0(1.1) | 113.7(0.8) | 117.0(1.0) | 118.0(1.3) |
| T2oz | 112.1(1.4) | 106.7(1.0) | 111.9(1.2) | 113.2(0.9) | 102.0(1.1) | 110.9(1.5) |
| T2mo | 109.2(1.0) | 104.0(1.0) | 111.7(1.4) | 112.8(1.4) | 107.0(1.0) | 112.1(1.0) |
| T2mz | 111.0(1.0) | 106.7(0.9) | 100.2(1.2) | 110.8(1.4) | 111.0(1.0) | 116.6(0.9) |
| | | | 31 kbar | | | |
| T1oo | 102.9(8) | 116.7(7) | 101.5(6) | 110.9(7) | 113.3(7) | 110.9(7) |
| T1oz | 97.6(7) | 118.7(7) | 94.5(6) | 115.1(7) | 117.0(7) | 111.9(7) |
| T1mo | 98.6(5) | 112.8(7) | 105.9(8) | 114.2(7) | 111.8(8) | 112.4(7) |
| T1mz | 106.2(6) | 114.2(8) | 102.2(7) | 110.6(8) | 113.4(8) | 110.1(7) |
| T2oo | 99.2(8) | 100.3(7) | 108.8(7) | 114.9(6) | 115.0(6) | 115.8(8) |
| T2oz | 109.2(8) | 102.3(7) | 111.7(8) | 114.1(6) | 105.6(6) | 114.0(9) |
| T2mo | 108.0(6) | 106.7(7) | 105.5(9) | 112.8(8) | 109.3(6) | 114.2(7) |
| T2mz | 114.5(6) | 103.2(7) | 104.5(8) | 110.4(8) | 107.8(6) | 116.5(7) |

TABLE 4b. T–O–T bond angles from $I\bar{1}$ refinements

| | 1 bar | 25 kbar | 31 kbar | | 1 bar | 25 kbar | 31 kbar |
|---|---|---|---|---|---|---|---|
| Oa1o | 138.3(3) | 132.5(1.7) | 138.1(1.1) | Oa1z | 137.3(3) | 139.2(1.7) | 136.0(0.9) |
| Oa2o | 124.4(3) | 122.4(1.1) | 121.3(0.7) | Oa2z | 124.3(3) | 126.2(1.0) | 127.2(0.7) |
| Oboo | 133.8(3) | 129.2(1.7) | 136.0(1.1) | Oboz | 133.8(3) | 137.4(1.4) | 122.8(0.9) |
| Obmo | 156.7(4) | 157.9(1.2) | 142.2(0.7) | Obmz | 155.4(4) | 153.0(1.3) | 170.7(0.8) |
| Ocoo | 132.1(3) | 130.2(1.1) | 129.6(0.7) | Ocoz | 130.6(3) | 130.2(1.1) | 131.9(0.7) |
| Ocmo | 131.1(3) | 135.2(1.4) | 128.0(0.9) | Ocmz | 128.7(3) | 125.7(1.4) | 129.1(1.0) |
| Odoo | 131.8(3) | 128.8(1.6) | 125.0(0.8) | Odoz | 129.5(3) | 129.8(1.5) | 129.7(1.0) |
| Odmo | 150.7(3) | 159.8(1.2) | 169.2(0.9) | Odmz | 149.6(3) | 143.0(1.3) | 135.1(0.7) |

3a) remain unchanged, consistent with the previously observed low compressibilities of the Al–O and Si–O bonds. Very little internal deformation of the tetrahedra is observed either; most O–T–O bond angles (Table 4a) remain the same. However, the longer Ca–O bonds do show compression (Table 3b), although the amount of splitting of the pairs of Ca sites remains about the same (Fig. 2b, 2e). Thus, between 1 bar and 25 kbar, compression within the anorthite structure is accommodated by reduction of Ca–O bond distances arising from small flexings of the T–O–T bond angles (Table 4b) between essentially rigid tetrahedra.

As noted in the previous section, the almost complete absence of *c* and *d* reflections from the diffraction pattern of anorthite at 31 kbar indicates that the structure above the phase transition approximates $I\bar{1}$ symmetry far more closely than the structure below it. Thus, although the refinements at 1 bar and 25 kbar represent "average" structures, the 31-kbar structure appears to have true $I\bar{1}$ symmetry. In particular, the scattering density at the Ca sites at 31 kbar (Fig. 2c, 2f) shows a single maximum at each site, indicating that no averaging process is being performed by refining an $I\bar{1}$ structure.

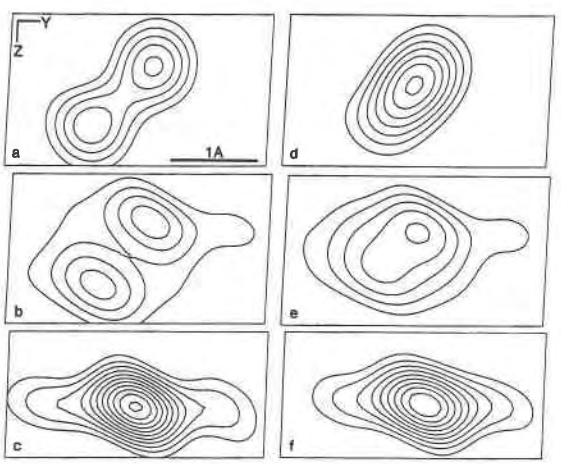


Fig. 2. Fourier sections of the scattering density at the Ca sites, using as coefficients unaveraged observed structure factors phased by calculated structure factors. The maps on the left are sections through the Mooo site at (**a**) 1 bar, (**b**) 25 kbar, and (**c**) 31 kbar. Those on the right are the Mzoo site at (**d**) 1 bar, (**e**) 25 kbar, and (**f**) 31 kbar. Note the change from split sites in the lower-pressure structures to single sites in the 31-kbar structure.

The same conclusion is reached upon examination of the structure of the tetrahedral framework at 31 kbar. The internal dimensions of the tetrahedra as represented by average T–O distances and O–T–O bond angles show no significant changes from the low-pressure structures. By contrast, significant changes in T–O–T bond angles are observed (Table 4b). The largest changes are those at Obmo, Obmz, Odoo, and Odmz, which correspond to the sites showing the largest deviations from $I\bar{1}$ symmetry in the low-pressure $P\bar{1}$ phase and therefore the largest differences in the T–O–T bond angles between pseudo-*I* related sites. Thus the differences in the structural parameters between the refinements at 1 bar and 25 kbar and the refinement at 31 kbar arise from the elimination of the averaging present in the low-pressure structure refinements. The removal of averaging is also reflected in the fact that the refined temperature factors of the framework atoms within the 31-kbar structure (Table 2c) are smaller than those of the corresponding sites in the lower-pressure structures (Tables 2a, 2b).

The results of the structural analyses therefore suggest that the phase transition may be described as a tilting of essentially rigid tetrahedra so as to bring the tetrahedra related by the pseudo-*I* symmetry into true equivalence. Since the T–O–T bond angles (Table 4b) that change most at the transition come to resemble at 31 kbar those at the *moi* and *mzi* oxygen positions of the $P\bar{1}$ structure at 1 bar (Wainwright and Starkey, 1971; Angel, Finger, and Carpenter, unpub. ms., 1988), rather than those at the *moo* or *mzo* positions, one may conclude that the majority of this tilting involves the *moo* and *mzo* tetrahedra.

## CONCLUSIONS

The main conclusion to be drawn from this structural study of anorthite is, of course, that the phase transition reported by Angel et al. (1988) is from a low-pressure $P\bar{1}$ structure to a high-pressure phase with true $I\bar{1}$ symmetry. It should be noted that attempts to refine the 31-kbar structure in a space group with lower symmetry such as *I*1 were unsuccessful, with all of the refined positions keeping to $I\bar{1}$ symmetry within the esd's.

The mechanism for the transition is the tilting of essentially rigid tetrahedra, apparently driven by a need to accommodate both the applied pressure and the large Ca cations with the cavities of the framework. Thus, although it appears that Ca–O bond lengths are appreciably shortened in the high-pressure structure, the volumes of

the cavities as defined by the eight closest oxygen positions remained the same, if not increased (Table 3b). The wide and relatively flat potential well within the cavities, which is typical of feldspars at ambient conditions, is replaced by a significantly sharper well at higher pressures as demonstrated by Figure 2.

Whether the high-pressure structure reported here is the same phase as that observed at temperatures in excess of 240°C must remain open to debate, as we have no reliable high-temperature structure determination with which to compare this work. The only such refinement of an anorthite at temperatures sufficiently in excess of the transition (Foit and Peacor, 1973) was carried out on $An_{98}$ material using a split-atom refinement. If indeed these are the same phases, the $P\bar{1}$-$I\bar{1}$ equilibrium phase boundary would have a negative $\delta P/\delta T$ slope, and the structural state of anorthite within the Earth's crust at even shallow depths would be $I\bar{1}$ (Angel and Ross, 1988). This conclusion would invalidate the suggestion of Grove et al. (1986) that this boundary should have a positive slope of several hundred degrees per kilobar in order for the inversion to drive the opening of the Hüttenlocher miscibility gap.

## Acknowledgments

I would like to thank Michael Carpenter of the University of Cambridge for supplying the material used in this study, and W. L. Brown, R. M. Hazen, H. Kroll, C. T. Prewitt, S.A.T. Redfern, and N. L. Ross for their reviews of the manuscript. This work was supported by NSF grants EAR86-18602 to C. T. Prewitt, EAR86-18649 to C. T. Prewitt and L. W. Finger, and by the Carnegie Institution of Washington.

## References cited

Adlhart, W., Frey, F., and Jagodzinski, H. (1980) X-ray and neutron investigations of the $P\bar{1}$-$I\bar{1}$ transition in pure anorthite. Acta Crystallographica, A36, 450–460.

Angel, R.J., and Ross, N.L. (1988) The high pressure phase transition in anorthites: Consequences for the phase relations of plagioclases. EOS, 69, 498.

Angel, R.J., Hazen, R.M., McCormick, T.C., Prewitt, C.T., and Smyth, J.R. (1988) Comparative compressibility of end-member feldspars. Physics and Chemistry of Minerals, 15, 313–318.

Carpenter, M.A. (1986) Experminental delineation of the "e" = $I\bar{1}$ and "e" = $C\bar{1}$ transformations in intermediate plagioclase feldspars. Physics and Chemistry of Minerals, 13, 119–139.

——— (1988) Thermochemistry of aluminium/silicon ordering in feldspar minerals. In E. Salje, Ed., Physical properties and thermodynamic behaviour of minerals. NATO ASI series C, 225, 265–323. Reidel, Boston.

Carpenter, M.A., McConnell, J.D.C., and Navrotsky, A. (1985) Enthalpies of ordering in the plagioclase feldspar solid solution. Geochimica et Cosmochimica Acta, 49, 947–966.

Facchinelli, A., Bruno, E., and Chiari, G. (1979) The structure of bytownite quenched from 1723 K. Acta Crystallographica, B35, 34–42.

Foit, F.F., and Peacor, D.R. (1973) The anorthite crystal structure at 410 and 830 °C. American Mineralogist, 58, 665–675.

Finger, L.W., and Prince, E. (1974) A system of Fortran IV computer programs for crystal structure computations. U.S. National Bureau of Standards Technical Note 854.

Grant, D.F., and Gabe, E.J. (1978) The analysis of single-crystal Bragg reflections from profile measurements. Journal of Applied Crystallography, 11, 114–120.

Grove, T.L., Ferry, J.M., and Spear, F.S. (1986) Phase transitions in calcic plagioclase: A correction and further discussion. American Mineralogist, 71, 1049–1050.

International tables for X-ray crystallography. (1974) Kynoch Press, Birmingham, England.

King, H., and Finger, L.W. (1979) Diffracted beam crystal centering and its application to high-pressure crystallography. Journal of Applied Crystallography, 12, 374–378.

Kirkpatrick, R.J., Carpenter, M.A., Yang, W.H., and Montez, B. (1987) $^{29}$Si magic-angle NMR spectroscopy of low-temperature ordered plagioclase feldspars. Nature, 325, 236–237.

Redfern, S.A.T., and Salje, E. (1987) Thermodynamics of plagioclase II: Temperature evolution of the spontaneous strain at $I\bar{1}$-$P\bar{1}$ phase transition in anorthite. Physics and Chemistry of Minerals, 14, 189–195.

Salje, E. (1987) Thermodynamics of plagioclase: I. Theory of the $I\bar{1}$-$P\bar{1}$ phase transition in anorthite and calcium-rich plagioclases. Physics and Chemistry of Minerals, 14, 181–188.

Wainwright, J.E., and Starkey, J. (1971) A refinement of the structure of anorthite. Zeitschrift für Kristallographie, 133, 75–84.

Wruck, B. (1986) Einfluss des Na-gehaltes und der Al,Si Fehlordnung auf das thermodynamische Verhalten der Phasenumwandlung $P\bar{1}$-$I\bar{1}$ in Anorthit. Dissertation, University of Hanover.

Manuscript received January 28, 1988
Manuscript accepted May 13, 1988